

**THE EFFECT OF IMPLANT ANGLE AND RESIST SHADOWING IN
SUBMICRON IMPLANT TECHNOLOGY**

LEE KANG HAI

UNIVERSITI SAINS MALAYSIA

2006

**THE EFFECT OF IMPLANT ANGLE AND RESIST SHADOWING IN
SUBMICRON IMPLANT TECHNOLOGY**

by

LEE KANG HAI

**Thesis submitted in fulfilment of the
requirements for the degree
of Master Degree**

JULY 2006

ACKNOWLEDGEMENTS

I would like to take this opportunity to acknowledge my university supervisor, Prof Dr. Kamarulazizi Ibrahim and my company supervisor, Mr. Thirumal Thanigaivelan, Manager of Implant Department, Silterra for their encouragement and supervision of my master project. To me, their guidance and advice is really the key to the accomplishment of this project.

I also would like to draw my appreciations to Silterra implant group such as my mentor Mohd Huzainy, Nor Shahril, Asrul, Thavanewaran, Teoh Whai Theik, Beh Chor Yeow, Johann Ong, Rajan, J.T. Lim, many other engineers, vendors and technicians for their useful technical support regarding ion implantation.

Besides that, special thanks to Silterra integration group especially, Andrew, Palaniviel, Soon Aik, Kai Sian and Hafizah for their advice and support during the project.

Of course I also in debt to Silterra HRD groups such as Ms Lena Tan, Mr. Abdullah bin Lin, Nor Asmah and Nor Shafarina for their support in managing the postgraduate internship program.

Last but no least, I would like to thank my lovely mom, sister and brother for giving their full support when I most need it.

TABLE OF CONTENTS

	Page
ACKNOWLEDGEMENTS	iii
TABLE OF CONTENTS	iv
LIST OF TABLES	vii
LIST OF FIGURES	viii
LIST OF PLATES	xiii
ABSTRAK	xiv
ABSTRACT	xvi
CHAPTER 1: INTRODUCTION	
1.0 Introduction to ion implantation and implant angle engineering	1
1.1 Well structure with channeled and dechanneled implant approach	3
1.2 Formation of the well structure by quad implant	4
1.3 Objective	5
1.4 Thesis Overview	6
CHAPTER 2: LITERATURE REVIEW	
2.0 Introduction	8
2.1 Review on the spatial variation in ion implantation	8
2.2 Review on the impact of implant tilt angle	10
2.3 Review on the CMOS device performance of 0° tilt approach to form retrograde well	15
CHAPTER 3: THEORY	
3.0 Introduction	18
3.1 Theory of ion implant process	18
3.1.1 Projectile and range theory (Ion stopping theory)	18
3.1.2 Monte-Carlo based SRIM	21
3.1.3 Ion implant process	22
3.1.4 Ion implant angle	24
3.1.5 Channeling effect in ion implant and relation with implant angle	26
3.2 Theory of ion implanter	28
3.2.1 Implanter fundamental	28
3.2.2 Batch processing implanter endstation	29

3.2.3	Geometrical design of spinning disk implanter	31
3.2.4	Cone angle in batch implanter	33
3.2.5	Spatial variation in high-energy implantation	36
3.3	Theory of ion implant metrology	38
3.3.1	Thermal wave system	38
3.3.2	Thermal wave as measurement of dopant profiles	40
3.4	Theory of device characterization	43
3.4.1	Reviews on CMOS well performance	43
3.4.2	Electrical characterization of the CMOS well	45
3.4.3	Source to drain subthreshold leakage (I_1)	46
3.4.4	PN Junction Reverse-bias current (I_2)	47
3.4.4.1	Junction capacitance	47
3.4.5	Parasitic vertical bipolar junction transistor (BJT) beta gain	48
3.4.5.1	Latchup in CMOS	49
3.4.5.2	Conditions for latchup	50
3.4.6	Interwell leakage (I_4 and I_5)	51
3.4.7	Characterization of interwell performance	52
3.4.8	Characterization of intrawell isolation	53
CHAPTER 4: EXPERIMENTAL SETUP		
4.0	Introduction	56
4.1	GSD200 HE implanter	56
4.2	Thermal wave system TP500	68
CHAPTER 5: DESIGN OF EXPERIMENT		
5.0	Introduction	72
5.1	Experiment for TW evaluation of the implant angle	72
5.1.1	Experiment flow	72
5.2	Experiment for electrical characterization of implant angle	72
5.2.1	Fabrication of Nwell and Pwell	72
5.2.2	Design of experiment	73
5.2.3	Electrical characterization	74
CHAPTER 6: RESULT AND DISCUSSION		
6.0	Introduction	76
6.1	TW analysis on different tilt for high-energy implantation.	76
6.1.1	TW analysis for single implant with different tilt angle	77

6.1.1.1	Correlation between lateral dopant profile uniformity and tilt angle	79
6.1.2	TW analysis for the beam incident of quad implant	84
6.1.2.1	TW analysis on the quad 7	86
6.1.2.2	TW analysis on quad 2	87
6.1.3	Dual implant process	89
6.2	Electrical characterization of the well formation for low tilt single implant and high tilt quad implant	92
6.2.1	Interwell isolation performance	93
6.2.2	Intrawell (well to well) isolation	97
6.2.3	Junction capacitance	100
6.2.4	Parasitic vertical bipolar junction transistor PNP beta gain, β_{pnp}	102
6.2.5	Characterization of other device performance	103
6.2.6	Optimized well implant angle	105
CHAPTER 7: CONCLUSION		
7.1	Summary	107
7.2	Future work	108
BIBLIOGRAPHY		
APPENDICES		
	Appendix A Experimental data and figures for TW analyses	109
	Appendix B SIMS simulation for the samples	115
	Appendix C Experimental data and figures for electrical analyses	118
REFERENCES		120
PUBLICATIONS		125

LIST OF TABLES

	Page
1.1 Quad implantation sequences	4
2.1 Wafer cut offsets form <100> plane	10
3.1 Illustrate the example of simulation programs	20
4.1 The maximum energy and beam current for Boron and Phosphorous implant	63
5.1 Implant conditions to form the Nwell and Pwell in this experiment	73
5.2 Nwell and Pwell implant conditions for the samples.	74
6.1 TW mean and σ for quad 2 implant	88
6.2 The improvement of TW sigma for dual implant process.	90

LIST OF FIGURES

		Page
1.1	The encroachment of well due to thick photoresist (PR) shadowing for tilted implant of different device dimension	2
1.2	Retrograde well formed by (a) high tilt dechanneled implantation and (b) channeling implantation	3
1.3	Formation of Nwell by (a) high tilt quad implant process (b) near 0° tilt implant process	5
2.1	Rs average and s as a function of implantation twist angle for 5° and 7° tilt angle. Quad implant process: B+, 5 keV, 4×10^{13} cm ⁻² ions/cm ² .	9
2.2	Doping profile for substrate lot number #1 to #5 in Table 2.1	10
2.3	a) SIMS depth profiles for B++, 540keV, 2×10^{13} cm ⁻² at various tilt angles. b) SIMS measurements and simulation results for P, 800keV, 3×10^{13} cm ⁻² atoms/cm ² , 0° twist with tilts at 0°, 0.2°, 0.4°, 0.6°, 0.8° and 1.3°. SIMS measurements were performed at the wafer centers. For 0° and 0.8° tilt, SIMS measurements were performed at wafer left and right positions from the 10mm wafer edges and consistent SIMS profiles across the wafers were obtained. Crystal-TRIM simulation result at 0° tilt is shown.	11
2.4	(a) Simulated net doping profiles n-well [7]. (b) Simulated net doping profiles p-well [7].	12
2.5	(a) Change in Vth for PFET and NFET as a function of implant angle error. (b) Isolation robustness for all implant and photoresist conditions investigated.	13
2.6	(a) Normalized Vth, (b) normalized Ion, and (c) normalized Ioff box plots for devices as a function of halo implant tilt angle. Normalization is with respect to mean values obtained from the nominal cell (0° tilt angle offset)	13
2.7	Implant angular dependence of threshold voltage for NMOS	14
2.8	SIMS profiles at center, left and right location (Qual-center, Qual-Left and Qual-Right) of a wafer for P, 400keV, 1.5×10^{13} ions/cm ² implanted using a dual setting of (α , β) of (0°, 1°) + (0°, -1°) on an HE 300mm implanter	15
2.9	Implant uniformity (in standard deviation of Rs) within 8-inch Wafer (after 900°C annealing) for (a) B+, 200keV (b) P+, 400keV.	16
2.10	Comparison of inter-well isolation characteristics between 0° tilt implantation and 7° tilt implantation	16
2.11	A ratio of junction leakage current at Vd =4V of 0° tilt implantation to that of 7° tilt implantation	17
3.1	Description of ion range R and projected range Rp.	19

3.2	Depth profile for 3 MeV Phosphorous	20
3.3	Doping profile by using SRIM simulation	21
3.4	Dose and energy requirement of ion implant process depending on the implantation application	23
3.5	The standard CMOS structure	23
3.6	(a) Definition of tilt (θ) and twist (Φ) (b) wafer orientation for <100> wafer	24
3.7	Different orientation of the silicon substrate	25
3.8	(a) the silicon density for tilt 0° (b) the silicon density for tilt 7° twist 22°	25
3.9	SIMS profiles of (a) 300keV Boron and (b) 600keV Phosphorous as a function of angle from the (100) direction	26
3.10	The critical angle (Ψ_c) for channeling and the distance of closest approach, r_{min} , of a channeled ion. (A) and (B) are the trajectories of a channeled ion ($\Psi < \Psi_c$) (C) is the trajectory of a dechanneled	27
3.11	Major sub-unit of ion implanter	28
3.12	The spinning disk endstation	29
3.13	Schematic of spinning disk endstation	30
3.14	(a) Mechanical scanning of spinning disk implanter (b) Illustrate the side view of spinning disk	30
3.15	The schematic diagram of the multi-wafer end station, showing definitions of α , β , and p . α is a rotation in the plane of the paper around the center of the wafer. β is a rotation orthogonal to α . p is the angle between the wafer pedestal and the plane of the disk. Note that $p = 5.0^\circ$ for the GSD200 HE implanter endstations. (b) This is the definition of γ and the calculation of γ_{min} and γ_{max}	31
3.16	Schematic of the notch position (δ) adjustment	32
3.17	Schematics of concave disk induced ion beam incident angle variation. (a) The rotation of disk is equivalent to rotating the beam to form a cone shape. (b) Illustration of incident angle variation. The beam scans along the trajectory AGB in the wafer with the incident angle varies from $\angle AQQ$ to 0° to $\angle GQB$.	33
3.18	A disk loaded with wafers. An arbitrary point P in wafer G can be expressed as P(x,y) in a X-Y coordinate with the wafer center G as the origin. The rotation of disk induced a maximum twist angle variation θ_M .	34
3.19	SIMS profiles for 320keV $1.0 \times 10^{13} \text{cm}^{-2}$ Phosphorous implant with different TW signal	36
3.20	Thermal wave contour maps	37
3.21	Example of TW profiles	37
3.22	Setup for thermal wave measurement of implanted silicon	38
3.23	Example of SIMS profile for Phosphorous implantation	41

3.24	Schematic basic CMOS structure	44
3.25	The vertical well profiles with the purpose of doping placement	44
3.26	Leakage current mechanisms of deep-submicrometer transistor	45
3.27	Illustrate the junction capacitance	47
3.28	Test structure cross section to form the vertical PNP BJT	49
3.29	Schematics of device cross section and equivalent circuit for latchup	49
3.30	Parasitic MOS transistors formed at the well edge in n-well CMOS. (IEEE 1987)	51
3.31	The layout and the test structure to characterize the (a) N+ to Nwell and (b) P+ to Pwell leakage and punchthrough voltage.	52
3.32	The layout and the test structure to characterize the (a) Nwell to Nwell and (b) Pwell to Pwell leakage and punchthrough voltage.	53
4.1	Schematic for the GSD HE implanter	57
4.2	Gas feed systems	58
4.3	Ion source of the NV-GSD HE implanter	59
4.4	Ionization process in the arc chamber	60
4.5	Electrode assembly	61
4.6	(a) Beam steering with axis X	62
	(b) Beam steering with axis Y	
	(c) Beam steering with axis Z	
4.7	Magnet analyzer of GSD HE implant system	63
4.8	LINAC (linear accelerator)	64
4.9	RLC circuit in GSD LINAC	64
4.10	High voltage electrodes oscillate at radio frequency, accelerating ions across each electrode gap	65
4.11	Resolving housing of GSD implanter	66
4.12	Faraday suppression	67
4.13	Basic structure for the TP500 system	69
5.1	Definition of Nwell1, Nwell2, Pwell1 and Pwell2 implant.	73
5.2	Illustrate the electrical characterization of the well for CMOS.	74
6.1	The priority of implant angle engineering	76
6.2	TW standard deviation across the wafer for different implant tilt angle	78
6.3	TWU mean for different implant tilt angle	79

6.4	(a) TW signal across the wafer (TW profile) for 320keV Phosphorous (2,0) implant (b) Implant tilt angle across the wafer for 320keV Phosphorous (2,0) implant (c) TW contour across the wafer for 320keV Phosphorous (2,0) implant	80
6.5	Tilt angle error across the wafer for different tilt angle setting on spinning disk implanter	82
6.6	Correlation between tilt angle error and TW standard deviation for P 320keV implant	83
6.7	(a) TW sigma for different quad angle (b) TWU mean for different quad angle	84
6.8	(a) TW profiles for the individual Phosphorous implant of quad 7 (b) Simulated and actual TW profiles for Phosphorous quad 7	86
6.9	Tilt angle error for individual implants of quad 2	88
6.10	Tilt angle variation for Phosphorus implant angle with (0°, 1°) and (0°, -1°)	90
6.11	N+ to Nwell (a) punchthrough voltage (b) leakage current roll-off for Pwell1 implant energy split with 220keV, 100keV and 180keV for W1U, W1T and W1L respectively	93
6.12	P+ to Pwell (a) punchthrough voltage (b) leakage current roll-off for Pwell1 implant energy split with 220keV, 100keV and 180keV for W1U, W1T and W1L respectively	93
6.13	Illustrate leakage current path from N+ to Nwell	94
6.14	N+ to Nwell (a) punchthrough voltage (b) leakage current roll-off for Pwell2 implant energy split with 140keV, 120keV and 100keV for W2U, W2T and W2L respectively	95
6.15	P+ to Pwell (a) punchthrough voltage (b) leakage current roll-off for Pwell2 implant energy split with 140keV, 120keV and 100keV for W2U, W2T and W2L respectively	96
6.16	Illustrate different Nwell profile encroachment for implant angle with (a) quad 5 and (b) tilt 2°	97
6.17	Nwell to Nwell (a) punchthrough voltage (b) leakage current roll-off between quad 5 split (Std) and tilt 2° splits (Tgt, W1U, W1T and W1L) for Nwell1 implant	98
6.18	Schematic showing the lateral encroachment of the Nwell	99
6.19	Illustration of the Nwell to Nwell punch through	99
6.20	Nwell to Nwell (a) punchthrough voltage (b) leakage current roll-off between quad 5 split (Std) and tilt 2° splits (Tgt, W1U, W1T and W1L) for Nwell2 implant	100
6.21	Junction capacitance for (a) NMOS and (b) PMOS	101
6.22	SRIM simulation Pwell for (a) Tgt and W1U samples (b) Std and W2L samples	102
6.23	Beta PNP gain for test structure with (a) 5µmX5µm and (b) 10µmX10µm	103
6.24	Id vs Ion curves for 0.13µm node (a) NMOS and (b) PMOS	104

6.25	V _{th} vs drive current, I _d for 10μmX0.13μm (a) NMOS and (b) PMOS	104
6.26	Proposed implant angle on well1 and well2 implant	105

LIST OF PLATES

	Page
4.1 Axcelis GSD200 implanter	56

KESAN SUDUT PENANAMAN DAN PEMBAYANGAN RINTANG TEKNOLOGI SUBMIKRON

ABSTRAK

Dengan adanya peningkatan teknologi bagi industri fabrikasi litar terkamil (IC) ke tahap 90nm dan seterusnya, masih terdapat isu yang perlu ditimbangkan untuk teknologi yang lebih rendah ($0.13\mu\text{m}$ dan $0.22\mu\text{m}$). Penskalaan litar terkamil secara lateral mengalami had apabila berhadapan dengan kesan *encroachment* pada profil akibat pembayangan rintang (resist shadowing) untuk proses penanaman telaga (well). Salah satu penyelesaian untuk masalah ini adalah dengan memacu sudut penanaman ion ke *normal regime* ataupun 0 darjah. Namun begitu, pendekatan ini akan mengakibatkan masalah saluran dopan (dopant channeling) yang serius. Maka, terdapat beberapa percubaan untuk mengaji kesan sudut penanaman ion dan pembayangan rintang ke atas teknologi sub-mikron. Tujuan kajian ini adalah untuk menentukan keberkesanan pendekatan baru untuk membentuk struktur telaga (well) dengan menggunakan penanaman bersudut hampir normal (hampir kosong darjah). Untuk mencapai tujuan ini, terdapat keperluan untuk mencari keseimbangan di antara saluran dopan dan pembayangan rintang bagi penanaman tenaga tinggi untuk sudut condong (tilt) rendah. Kajian ini akan mengfokus kepada penanaman tenaga tinggi sudut condong rendah kerana regim penanaman ini mempunyai beberapa isu serius pada saluran dopan dan pembayangan rintang. Semua proses implantasi dalam eksperimen telah dijalankan menggunakan sistem *implanter GSD* yang menggunakan *spin disk endstation*. Terdapat dua eksperimen untuk menganalisis kesan sudut penanaman keatas teknologi submikron. Eksperimen pertama adalah untuk menganalisis keseragaman implantasi ion dengan tujuan mencari sudut penanaman yang optimum. Dalam kajian ini, semua sampel telah disediakan dengan menjalankan implantasi single dan quad dari sudut 0 hingga 7 darjah. Pencirian keseragaman penanaman dilakukan dengan pengukuran gelombang termal (thermal wave) pada sampel. Bagi penanaman tenaga tinggi

sudut rendah, keseragaman penanaman ditentukan oleh ralat sudut bim penanaman. Dari segi keseragaman penanaman, kecondongan sudut penanaman 2 derajat ke atas telah dicadangkan untuk proses penanaman *single* (single implant). Manakala quad 4 dan quad 5 telah dicadangkan untuk penanaman *quad* (quad implant). Eksperimen seterusnya melibatkan mengfabrikasi struktur telaga yang baru dengan menggunakan penanaman 2 derajat untuk menghasilkan profil dopan telaga yang menyalur (channeled well profile). Prestasi *device* telah dibandingkan dengan struktur telaga konvensional yang mempunyai profil dopan yang tidak menyalur (dechanneled well profile) yang telah difabrikasi menggunakan penanaman quad 5. Berasaskan analisis pada ujian elektrik dalam eksperimen ini, sudut penanaman telaga (well implant) baru yang mana masa kitaran penanaman lebih singkat berbanding dengan penanaman *quad* telah dicadangkan untuk memperbaiki prestasi *N+ to Nwell isolation* tanpa mengganggu I_d/I_{off} dan V_{tlin}/I_d MOSFET. Ini boleh tercapai dengan sudut 5 derajat pada penanaman telaga dalaman (deeper well implant) dan sudut 2 derajat pada penanaman telaga (well) pada kawasan *field oxide*. Kajian ini menunjukkan potensi penggunaan struktur well dengan profil yang menyalur untuk meningkatkan prestasi *isolation*. Namun begitu, ini masih perlu mengoptimumkan tenaga dan dos penanaman.

THE EFFECT OF IMPLANT ANGLE AND RESIST SHADOWING IN SUBMICRON IMPLANT TECHNOLOGY

ABSTRACT

As the integrated circuit (IC) fabrication industry gears up to volume manufacturing of 90nm technology node and beyond, there are issues still need to be addressed at the lower technology nodes such as 0.13 μm and 0.22 μm . The lateral scaling has faces limitation in dealing with the profiles encroachment due to resist shadowing for well implant process. Driving the ion implant angle to near normal regime is a potential solution for the above concern. Nevertheless, this approach will lead to severe dopant channeling. Thus, there is an interest to study the impact of implant angle and resist shadowing on sub-micron technology. The goal for this work was to determine the feasibility of a novel approach to forming a well with near 0° tilt implantation. To achieve this, there is a requirement to find a compromise between dopant channeling and resist shadowing for the high-energy implantation in low tilt angle regime. This study will focus on low tilt angle high-energy implantation since this implant regime has more severe issues on the resist shadowing and dopant channeling. All implant processes in the experiments were performed by spin disk endstation GSD batch implanter system. There are two experiments to evaluate the impact of implant angle. The first experiment is to evaluate the uniformity of the dopant profile across the wafer (implant uniformity) with the intention to find the optimum implant tilt angle with acceptable implant uniformity. In this work, all sample wafers have been prepared by performing single and quad implantations with implant angle 0° to 7°. The characterization of implant uniformity has been done by thermal wave measurement on the sample. For low tilt high-energy implantation, the implant uniformity is dominated by the implant beam angle error. In terms of the dopant profile uniformity across the wafer, tilt 2° or higher tilt angle implant has been proposed for single implant process. Meanwhile, quad 4 and quad 5 have been proposed for quad implant. The second experiment in this work involves fabrication of the novel well structures with tilt 2° implant to create

channeled well doping profile. The device performance is compared with the conventional well structures with dechanneled doping profiles, which were fabricated by quad 5 implant. Based on the analysis on the transistor electrical data, a novel implant angle scheme with improved cycle time has been proposed. The proposed scheme improves the N+ to Nwell isolation performance without deteriorating I_d/I_{off} and V_{tlin}/I_d characteristics of MOSFET. This can be achieved by performing high tilt quad 5 at the deep well region and low tilt 2-degree implant at the field oxide region. The work indicates the potential of implementing the well with channeled profiles for the improvement of isolation performance with further optimization of the dose and energy.

CHAPTER 1

INTRODUCTION

1.0 Introduction to ion implantation and implant angle engineering

In the complementary metal oxide semiconductor (CMOS) fabrication process, ion implantation is primarily used to add dopant ions (most often selectively) into the surface of silicon wafers. The applications of the ion implantation process are source/drain formation, threshold voltage adjustment, well formation, channel-stop implantation, punchthrough stopper implantation and graded source and drain formation in CMOS fabrication [1]. Each implant application can be achieved by controlling the dosage, beam current, implant energy, angle and dopant species of ion implant process.

The fast pace of the device shrinkage has put stringent control on the implant process to provide different junctions for different implant steps mentioned earlier. This has created a whole new topic of interest called the “Junction Engineering”. The junction engineering has becoming more critical as the device continues to shrink. The implant angle is one of the critical factors affecting the junction.

There will be different criteria of the implant angle depending on the implant applications. Large Angle Tilt Implants (LATID) has been introduced purposely in order to reduce short channel effect (SCE) and punch through effect. Meanwhile, source and drain implant (SD implant) require implant angle that creates shallow and abrupt dopant profiles [2].

Well implant application, which involves high-energy implant, requires thick photoresist to mask the penetration of high-energy ions. In most cases, the ions

will be implanted into a wafer at a tilt angle to minimize channeling. It is common practice to implant with 7° tilt angle to avoid the dopant channeling. However, ion implant with tilt 7° is no longer the best implant angle due to the shadowing from photoresist.

The shadowing creates shadow regions (lateral encroachment) of the well profile as shown in fig 1.1 [3-6]. This lateral encroachment is relatively larger compare to the CMOS well for smaller device (see fig 1.1) and creates a barrier for device miniaturization. By reducing tilt implant angle towards 0° , the interwell isolation can be improved by reducing the lateral diffusion of the well dopant profile [7].

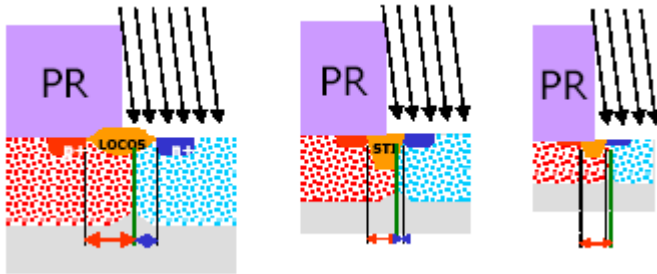


Fig 1.1 The encroachment of well due to thick photoresist (PR) shadowing for tilted implant of different device dimension [3]

Another concern in the junction engineering for well implant is the control of implant angle [8, 9]. The process control of implant angle highly depends on the ion beam scanning and wafer holder design of the implanter. For batch processing implanter where the wafers will put on a spinning disk (the spinning disk implanter will be reviewed in Chapter 3), the implant beam angle will deviate from the actual direction due to space charge and cone angle effect [9-15]. Since implant angle will affect the doping profile, any change in beam angle across the wafer may affect the implant uniformity. The uniformity of the doping profile across the wafer, as spatial variation of doping dopant across the wafer [11] is dependent on the implant angle setting [15]. Thus, proper setting of the implant angle is crucial for best implant uniformity across the wafer.

The issues above mentioned indicate that the implant angle engineering is a critical part of the junction engineering. Any improvements in the implant angle control will lead to dopant uniformity improvement, which will result in enhanced device performance and improved yields.

1.1 Well structure with channeled and dechanneled implant approach

As stated in section 1.0, higher implant angle* for well implants will lead to severe “mask edge shadowing”. The near 0° tilt well implant has been proposed as the solution to this issue [7].

It is known that channeling will occur at near 0° tilt angles [7]. Thus, conventional high tilt angle and high-energy well implantation will create abrupt doping profile with less dopant channeling. This will result in dechanneled well structure with a steep retrograde well. The proposed methodology discussed in this project is to form the well with uniform channeled doping profile and result in channeled well [16].

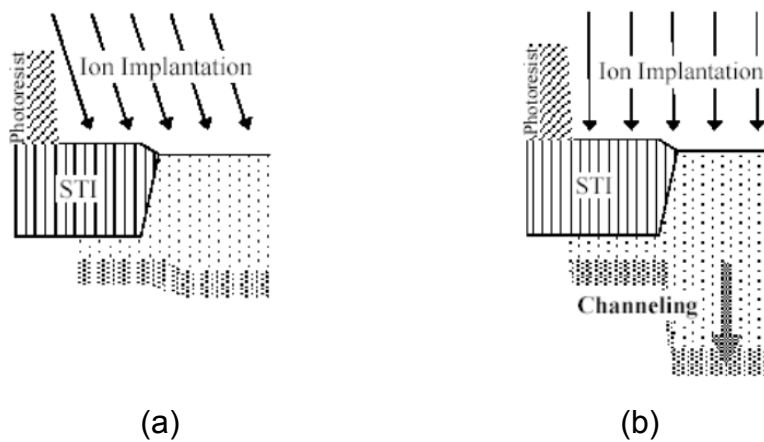


Fig 1.2 Retrograde well structure formed by (a) high tilt dechanneled implantation and (b) channeling implantation [16]

Fig 1.2(a) shows a conventional well structure with dechanneled profiles under STI (shallow trench isolation) and active region by tilting the implant angle

* High tilt angle is defined as the tilt angle higher than tilt 3° in this thesis

high enough to non-channeled regime. The proposed well structure in fig 1.2(b) requires 0° or near 0° implant to reduce the impact of resist shadowing. Fig 1.2 (b) shows the channeled profiles under active region and dechanneled profiles under STI. Low tilt implant in the high channel regime will create channeled doping profiles in the active region. Under the STI region, the implanted ions show dechanneled behavior because the STI oxide acts as the screen oxide to scatter the implanted ions [16].

In some cases, well implant with high tilt angle is performed in quad mode, which is known as quad implant process.

1.2 Formation of the well structure by quad implant

Quad implant process is a chain of four implants, each with one quarter of the dose. The implant angles will be at the same tilt, but 90° apart in twist. The quad implant angle for the disk implanter NV-GSD200 HE implanter (the model of implanter used in this work) will consist of (α, β) , $(-\beta, \alpha)$, $(\beta, -\alpha)$ and $(-\alpha, -\beta)$ all with quarter of total dosage, where α and β are angles in degree (see table 1.1).

Table 1.1 Quad implantation sequences [17].

Step No.	Tilt	Twist	Alpha	Beta
Q_1	θ	$\phi + 90^\circ$	α	$-\beta$
Q_2	θ	ϕ	$-\beta$	$-\alpha$
Q_3	θ	$\phi + 270^\circ$	$-\alpha$	β
Q_4	θ	$\phi + 180^\circ$	β	α

In this thesis, quad 1 will consist of 4 implant steps with angle $(1,0)$, $(0,1)$, $(-1,0)$ and $(0, -1)$. Meanwhile, quad 7 will consist of 4 implant steps with angle $(7,0)$, $(0,7)$, $(-7,0)$ and $(0, -7)$.

The quad implant can be used to form the symmetrical well of a standard CMOS as shown by fig 1.3(a) below. The near 0° tilt well implant approach in fig 1.3(b) will form a novel channeled well (see section 1.1) [14].

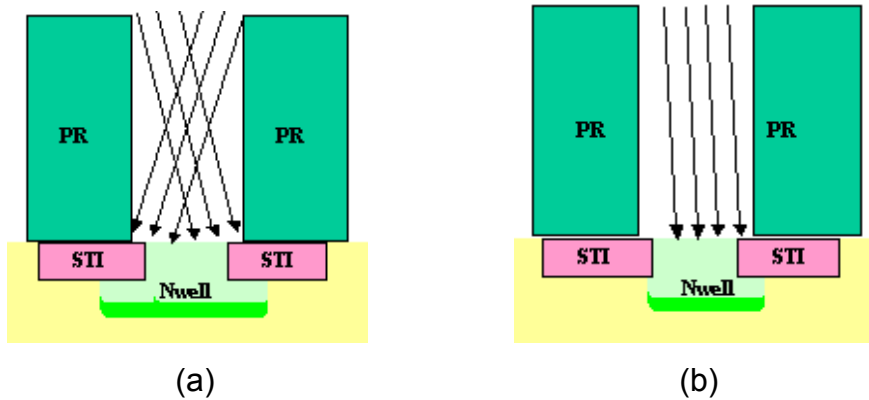


Fig 1.3 Formation of Nwell by (a) high tilt quad implant process (b) near 0° tilt implant process

The symmetrical well profiles encroachment of quad implant can solve the asymmetry of device performance due to photoresist shadowing [14]. However, the concern of the encroachment of well profile still exists if the quad implant involves high tilt angle. Thus, there is a requirement to lower the implant tilt angle to reduce the dopant profiles encroachment.

1.3 Objective

The intention of this work is to study the feasibility of forming a CMOS well with near 0° tilt high-energy implantation by using batch implanter with spinning disk endstation design. To achieve this, experiments have been carried out in order to evaluate the implant uniformity across the wafer for high-energy implant with different tilt angle and evaluate the device performance for the well with channeled and dechanneled doping profiles.

The objectives of this work can be summarized as following:

- To find the high-energy implant tilt angle with the optimum dopant profile uniformity across the wafer

- To evaluate the device performance for well implant with near 0° tilt and high tilt quad implant
- To fabricate a MOSFET with improved interwell isolation performance.

1.4 Thesis Overview

This thesis is divided into 7 chapters. The first chapter is the introduction to the control of implant angle for high-energy implant. In this chapter, the motivation and objective of this project are stated.

Chapter 2 is the literature review. The technical challenges and issues on low tilt angle for high-energy implant application as well as the history of previous works on the implant angle study are discussed. The implant angle control has been addressed. Apart from this, the device performance of 0° tilt approach to form the well is reviewed.

Chapter 3 reviews the fundamental concept of ion implant angle and dopant channeling. This chapter also discusses the endstation design for spinning disk implanter, cone angle effect and angle variation arising from it. In addition, description on the implant metrology theory (thermal wave) is reviewed. Then, the electrical characterization of CMOS well will be stated (test method and test structures for interwell isolation, intrawell isolation, parasitic junction capacitance, and parasitic bipolar beta gain).

Chapter 4 is the experimental setup where the tools such as ion implanter and the metrology used in this project will be stated. The specifications of the equipment setup were addressed as well.

Chapter 5 discusses the methodology of the experiment. The design of the experiments in this work will be shown. The experimental works can be generally

divided to thermal wave analysis on bare-wafers for implant profile uniformity evaluation and the comparison of the device performance for well implant with low tilt single implant and high tilt quad implant.

The experimental results will be discussed in Chapter 6. The early part of this chapter will evaluate the implant profile uniformity for different implant angle. The factor that dominates the implant profile uniformity across the wafer was stated. Then, the impact on dopant channeling on the CMOS well will be discussed. Based on the analysis in this chapter, optimum implant angles for well implant process will be proposed. The device performance for the MOSFETs, which were fabricated with the implant angle proposed in the first experiment will be shown as well.

The conclusion and the future work of thesis research are presented in Chapter 7. Meanwhile, other experimental data can be referred in Appendices.

CHAPTER 2

LITERATURE REVIEW

2.0 Introduction

This chapter covers the literature review of earlier works done on ion implant angle and shadowing effect. The chapter is split into three sections. First section covers the spatial variation in ion implantation from disk implanters. Second section goes over the impact of tilt angle error on the device performance. The third section reviews the 0° tilt approach to form the well.

2.1 Review on the spatial variation in ion implantation

As mentioned in chapter1, the spatial variation (non-uniformity) in the well dopant profiles [10] is the main challenge in implant angle engineering to perform the near 0° tilt well implant. This non-uniformity may present itself as a tilt, beam divergence, beam micro non-uniformity, photolithography, or even crystal cut error [19]. It has been reported that the non-uniformity of high-energy batch implantation is mainly contributed by the beam angle variation from batch implanter [10].

There are abundant literatures [8,9,11,20 - 22] emphasizing the requirement of implant angle control of the single wafer processing implant. This papers reported the limitation of the batch processing implanter to produce the uniform channeled doping profiles in the low tilt implant regime due to their beam angle accuracy from cone angle effect from the spinning disk endstation. Even though the batch implantation (with spinning disk endstation) has disadvantage on the accuracy of the beam angle, the dual tilt spinning disk endstation of batch implanter allows a fast adjustment of wafer tilt and twist angles and provides a high throughput for a quad implantation as is proposed by Axcelis technology.

Studies have been done to reduce the spatial variation dopant profile [8,9,17]. The implant angle study by Serguei Kondratenko [17] on low energy Boron quad implant has reported that tilt 7° twist 45° ($(\alpha,\beta) = (4.95^\circ, 4.95^\circ)$) can reduce the spatial variation and dopant channeling. This implant condition has resulted in a relatively high sheet resistance (R_s), indication of reduced channeling, and low standard deviation of R_s which is an indication of reduced spatial variation as shown in fig 2.1.

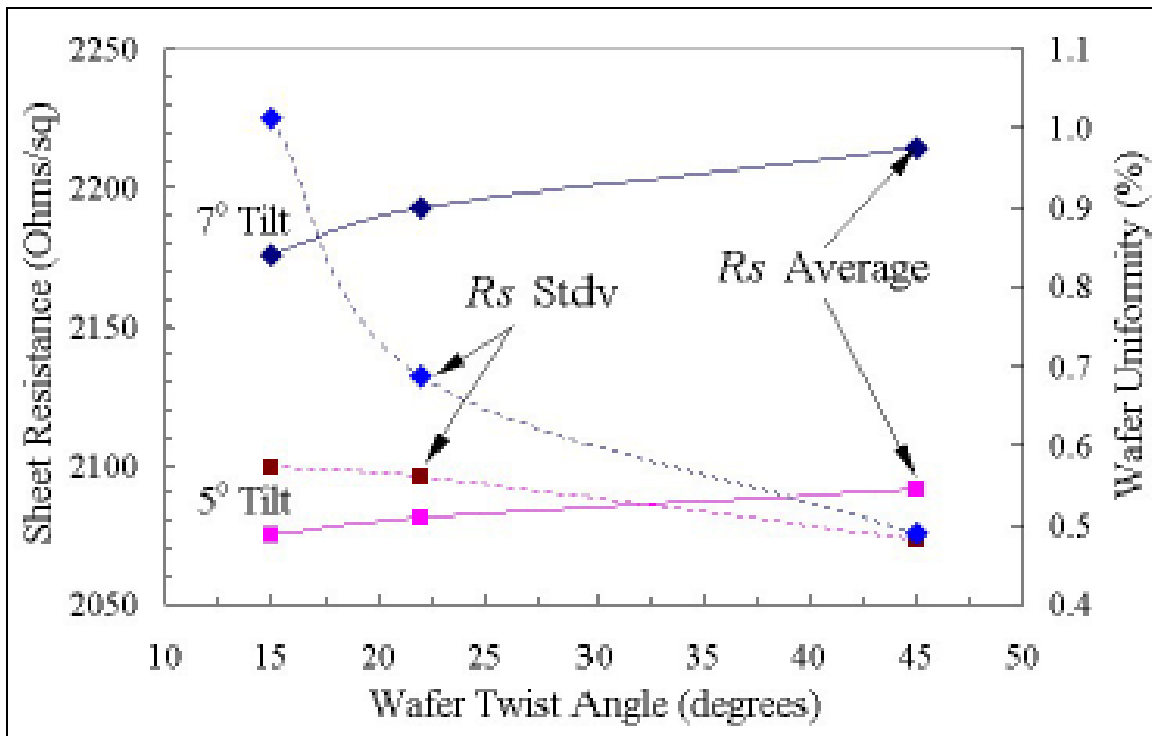


Fig 2.1 R_s average and standard deviation as a function of implantation twist angle for 5° and 7° tilt angle. Quad implant process: B+, 5 keV, 4×10^{13} ions/cm² [17].

It has also been reported that the wafer cut error will contribute to the incident beam angle error [10], which is tabulated in table 2.1 (see fig 2.2 for the variation of doping profiles between different substrate batches). The wafer cut error only lead to the wafer-to-wafer doping profiles variation and not the main root cause of the spatial variation across wafer.

Table 2.1 Wafer cut offsets form <100> plane [10].

substrate lot number	Θ – Tilt angle from <100> [degree]	Φ – Twist angle from notch [degree]
1	0.300	-45.4
2	0.725	66.4
3	0.300	-45.4
4	0.360	-20.7
5	0.506	20.5

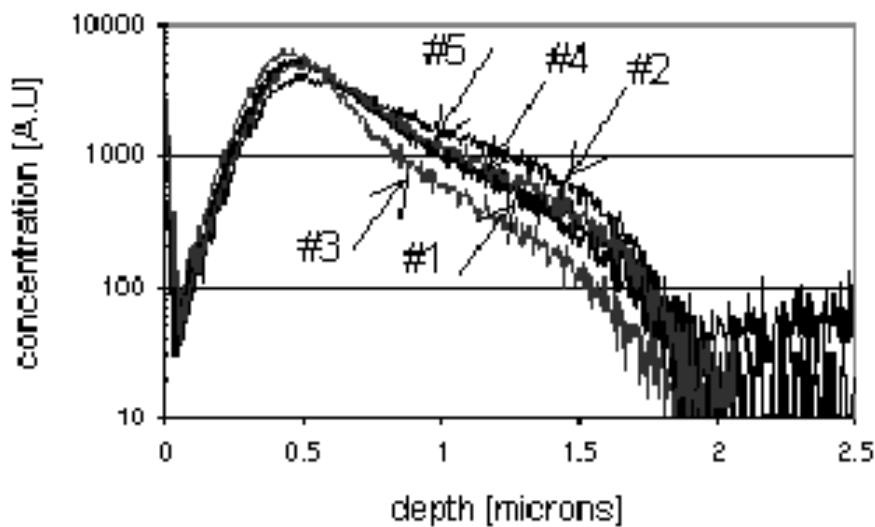


Fig 2.2 Doping profile for substrate lot number #1 to #5 in Table 2.1 [10].

2.2 Review on the impact of implant tilt angle

The impact of the small angle change on the shape of doping profiles has been reported [8]. The sensitivity of the profile shape to angles will rise with increasing ion energy [23]. Apart from this, comprehensive SIMS analyses also been performed on the low tilt high-energy implant regime [24]. Based on the SIMS analyses [24], there was a significant variation of the profile shape for the implant tilt lower than 1° (see fig 2.3(a) and fig 2.3(b)).

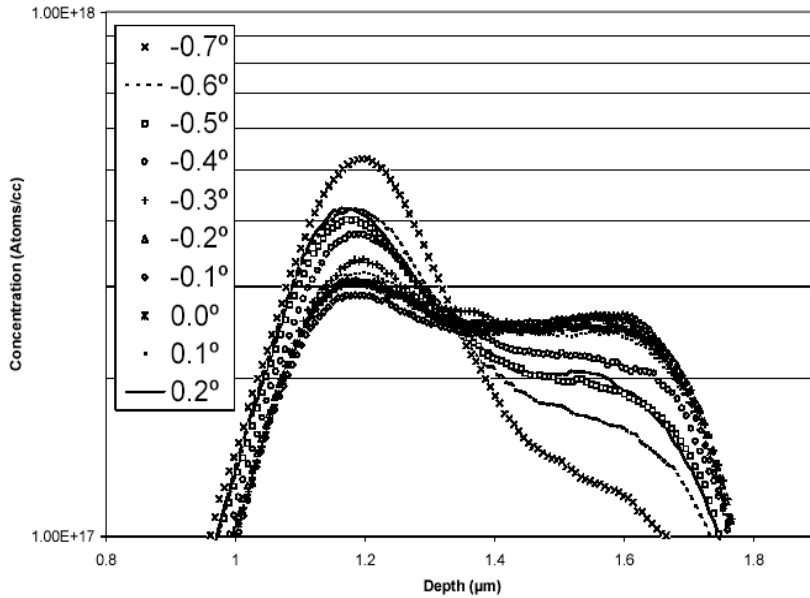


Fig 2.3 a) SIMS depth profiles for B⁺⁺, 540keV, $2 \times 10^{13} \text{ cm}^{-2}$ at various tilt angles [8].

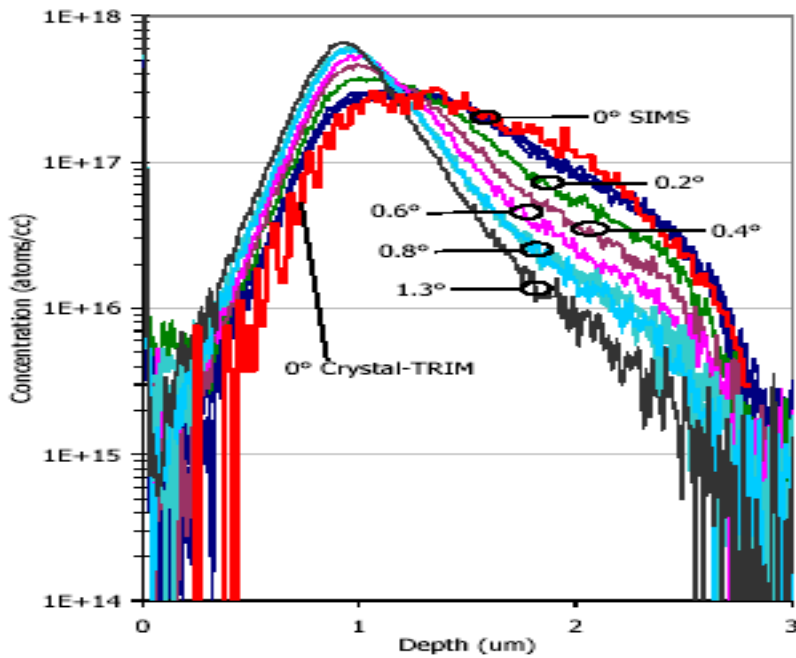


Fig 2.3 b) SIMS measurements and simulation results for P, 800keV, $3 \times 10^{13} \text{ atoms/cm}^2$, 0° twist with tilts at 0°, 0.2°, 0.4°, 0.6°, 0.8° and 1.3°. SIMS measurements were performed at the wafer centers. For 0° and 0.8° tilt, SIMS measurements were performed at wafer left and right positions from the 10mm wafer edges and consistent SIMS profiles across the wafers were obtained. Crystal-TRIM simulation result at 0° tilt is shown [24]

The well profiles (see fig 2.4(a)-(b)) has also been simulated [7] to study their impact on V_{th} and N^+ to Nwell isolation by using TSUPREMIV. For processes with 0° tilt well implants, beam angle variations $<1.0^\circ$ significantly alter the shape of typical n-well and p-well doping profiles (see fig 2.4(a)-(b)), V_{th} (see fig 2.5(a)) and interwell isolation performance (see fig 2.5(b)) compare to quad 3 well implants.

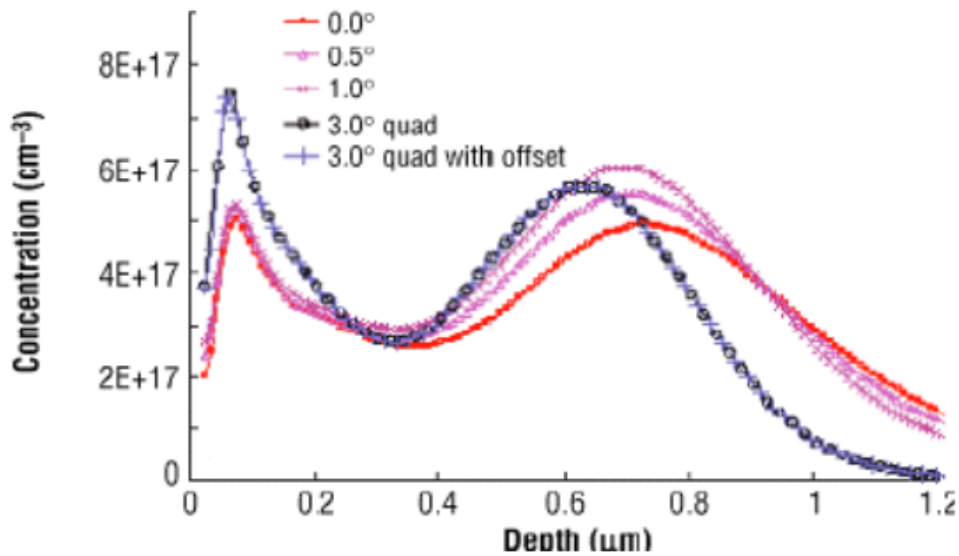


Fig 2.4 a) Simulated net doping profiles n-well [7].

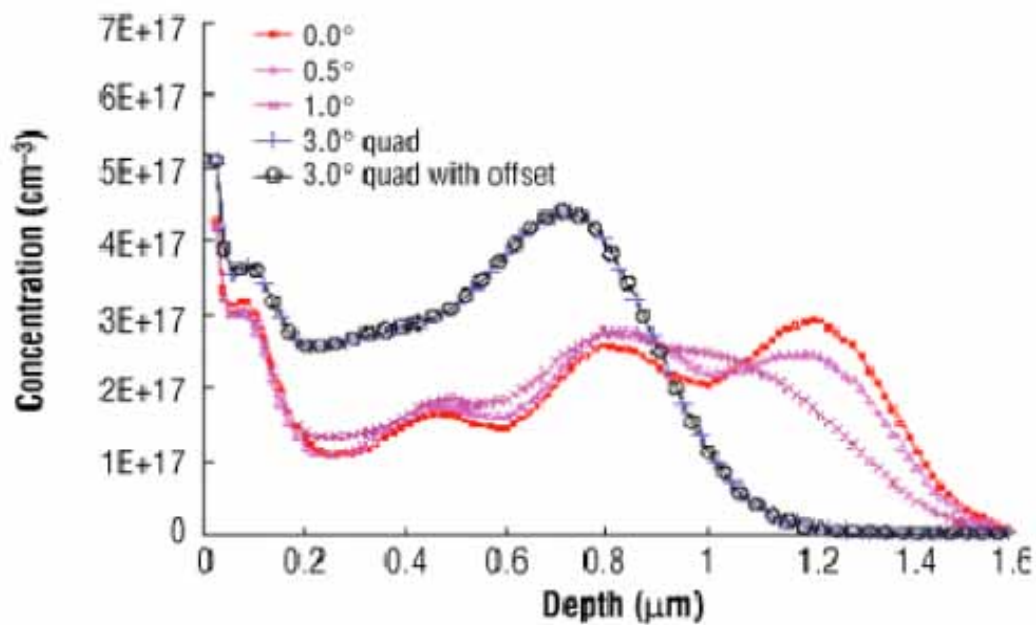


Fig 2.4 b) Simulated net doping profiles p-well [7].

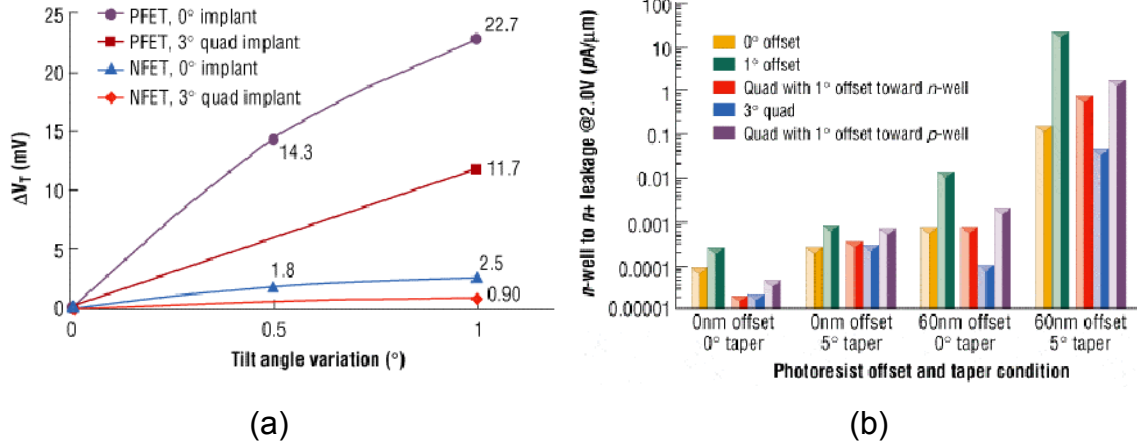


Fig 2.5 (a) Change in V_{th} for PFET and NFET as a function of implant angle error. (b) Isolation robustness for all implant and photoresist conditions investigated [7].

The tilt angle variation of the high tilt halo implant also induces significant impact on the device performance [25, 26]. The angle error [27] on the halo implant may induce significant effect on the threshold voltage (V_{th}) (see fig 2.6(a)), drive current (I_d) (see fig 2.6(b)) and off state current (I_{off}) (see fig 2.6 c)) for 0.14μm CMOS transistor.

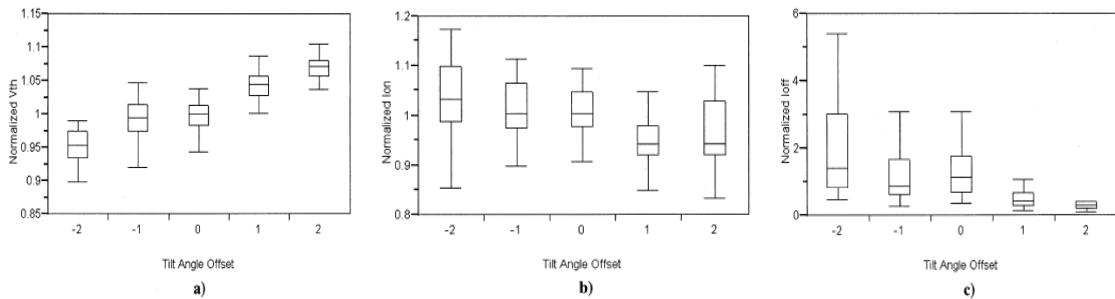


Fig. 2.6 (a) Normalized V_{th} , (b) normalized I_{on} , and (c) normalized I_{off} box plots for devices as a function of halo implant tilt angle. Normalization is with respect to mean values obtained from the nominal cell (0° tilt angle offset) [27].

Then, the dependence of depth profile and threshold voltage on tilt and twist angle has been investigated with a resolution of 0.05° using a stencil mask ion implanter that has less than 0.1° parallelism of ion beam [28]. By controlling beam parallelism to less than 0.1°, the deviation due to the channeling phenomena

should be negligible (refer to fig 2.7 for the impact of implant angle on the threshold voltage for NMOS).

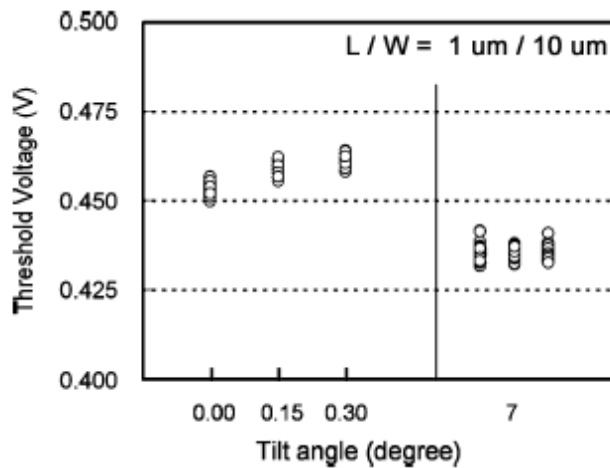


Fig 2.7 Implant angular dependence of threshold voltage for NMOS [28]

Apart from that, the sensitivity of implant angle has been summarized in the communicated point of views of high energies implants used for device isolation [25]. High energy implant is sensitive to implant angle where the implanted profiles may be significantly modified for small angle variations (below 0.8° [26], 0.6° [29] according to ion specie and beam energy). Device isolation analysis with 1.5 MeV vertical phosphorus implants showed that tilt angle variation has to be kept below 0.4° to not significantly modify isolation performance of aggressive design [30,31].

After the angle variation due to cone angle effect (see section 3.2.4 in Chapter 3) of the batch implant system was well recognized as the root cause of the implant non-uniformity, Axcelis technology has proposed the practices to reduce the cone angle effect by proper selection of implant angle (α, β and δ (refer to Chapter 3 for the definitions)) [32]. Apart from this, there is another method for reducing across-wafer spatial variation of dopant profiles on Axcelis' GSD implanter family by performing 0 degree dual-position implants [15]. This is able to produce uniform implant even on the 300mm wafer (see fig 2.8).

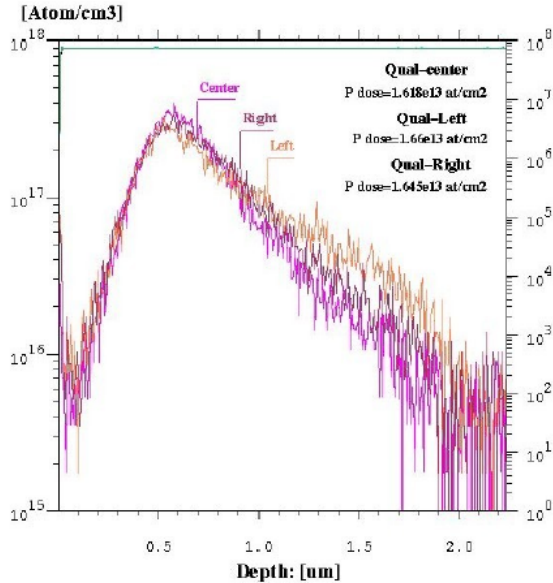


Fig 2.8 SIMS profiles at center, left and right location (Qual-center, Qual-Left and Qual-Right) of a wafer for P, 400keV, 1.5×10^{13} ions/cm² implanted using a dual setting of (α, β) of $(0^\circ, 1^\circ) + (0^\circ, -1^\circ)$ on an HE 300mm implanter [15].

2.3 Review on the CMOS device performance of 0° tilt approach to form retrograde well

Simulation study has been performed on the 0° tilt approach to form the retrograde well [32]. Based on the simulation, 0° tilt implantation is estimated to improve inter-well isolation by 0.2μm compared with 7° tilted implantation for 0.1μm retrograde well process. This retrograde well technology is indispensable for inter-well isolation in 0.1μm node. The technical challenge of performing near 0° tilt well implant approach by using batch implanter series has been reported due to their relatively poor dopant profiles uniformity within the wafer (see fig 2.9 for the implant uniformity of batch implantation with different tilt angle) [32].

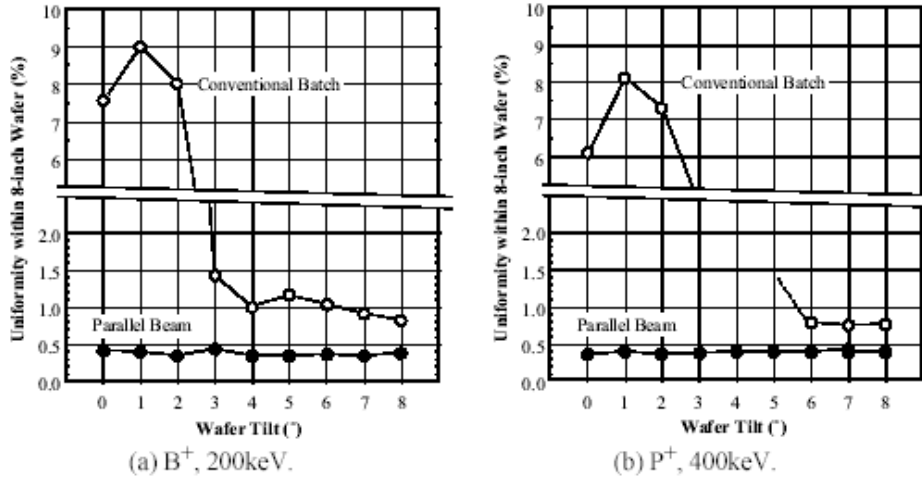


Fig 2.9 Implant uniformity (in standard deviation of R_s) within 8-inch Wafer (after 900°C annealing) for (a) B^+ , 200keV (b) P^+ , 400keV [32].

Another work that studied the device performance on the 0° well implant approach by using parallel beam implanter [16] reported that 0° channeling implantation with thin screen oxide can reduce both junction capacitance and junction leakage current without deteriorating a characteristic of MOSFETs. The improvement of 0° tilt implant on inter-well isolation leakage roll-off has been shown in fig 2.10 and junction leakage in fig 2.11 compare to 7° tilt implant.

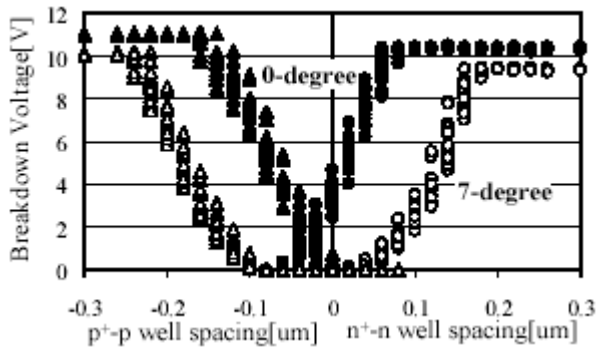


Fig 2.10 Comparison of inter-well isolation characteristics between 0° tilt implantation and 7° tilt implantation [16]

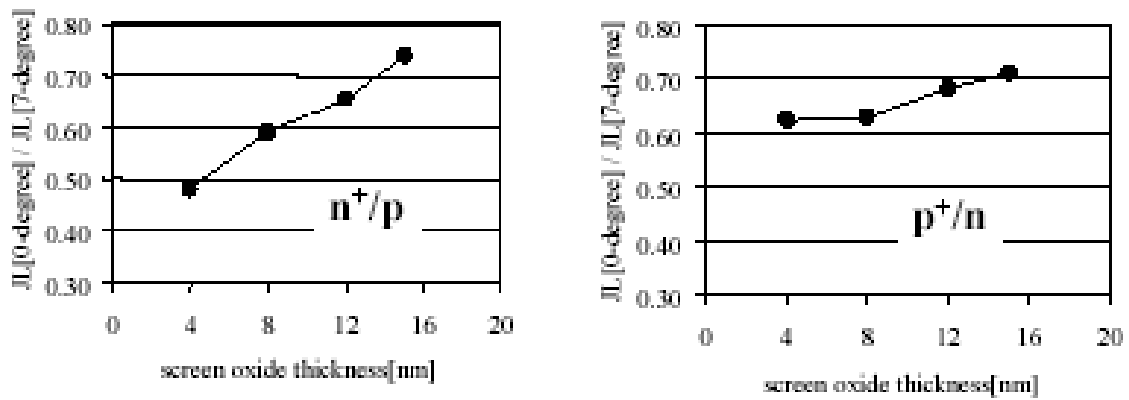


Fig 2.11 A ratio of junction leakage current at $|V_d|=4V$ of 0° tilt implantation to that of 7° tilt implantation [16].

As reviewed in this chapter, extensive study has been carried out on the near 0° tilt well implant by using single wafer processing implanter with parallel beam control system. However, no study has been reported on the capability of batch implanting process to form the well with near 0° tilt implant approach.

This work will focus on the study for the spatial variation of well implant process by the high-energy batch implanter. Subsequently, the device performance of the $0.13\mu\text{m}$ CMOS well with quad well implant and near 0° tilt well implant approaches were studied.

CHAPTER 3

THEORY

3.0 Introduction

This chapter is divided into four sections, which are theory of ion implant process, theory of ion implanter, theory of ion implant metrology and theory of device characterization. Theory of ion implant process covers ion stopping theory and channeling effect in ion implantation. Then, the fundamental of implanter, endstation design of spinning disk batch implanter and the cone angle effect in batch implanter are reviewed in the theory of ion implanter. The theory of ion implant metrology reviews the metrology to determine the spatial variation of dopant profiles. At the end of this chapter, the electrical characterizations of the isolation performance of the CMOS well are reviewed in the theory of device characterization.

3.1 Theory of ion implant process

3.1.1 Projectile and range theory (Ion stopping theory)

When an energetic ion moves through a solid, the kinetic energy of the ion is transferred to the lattice through the columbic interaction in nuclear collision with the lattice nuclei and with the electron around the lattice atoms [36]. The energy loss per unit length due to nuclear collision is called the nuclear stopping power $S_n(E)$, and the electronic stopping power $S_e(E)$ for electrons. The total distance of ion traveled in target is the range. The penetration depth of the implanted ion along the implantation direction is known as the projected range (R_p) as shown in fig 3.1 below.

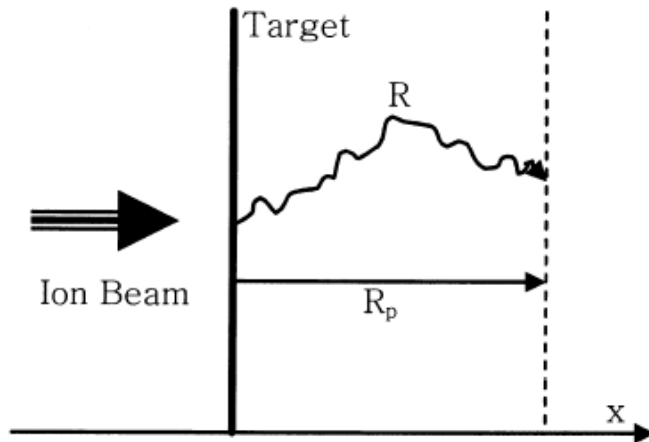


Fig 3.1 Description of ion range R and projected range Rp.

The rate of energy loss can be expressed by equation 3.0 as following [1]

$$-\frac{dE}{dx} = N[S_n(E) + S_e(E)] \quad (3.0)$$

where,

E = energy of the ion at a point x along its path,

N = atom density

The negative sign means that the energy decreases with depth due to the collision and the columbic interaction. The range can be obtained by integrating equation 3.0 with respect to energy as expressed by equation 3.1 [1]

$$R = \int_0^R dx = \frac{1}{N} \int_0^{E_0} \frac{dE}{S_n(E) + S_e(E)} \quad (3.1)$$

However, the actual implanted dopant depth, R will not be exactly as predicted by equation 3.1 but will be distributed statistically as the doping profiles in fig 3.2 below.

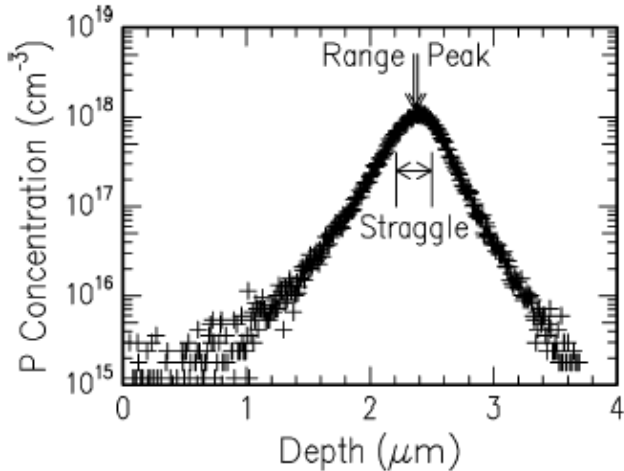


Fig 3.2 Depth profile for 3 MeV Phosphorous [14]

The dopant distribution (doping profiles) can be represented by Pearson IV distribution with four moments (parameters to represent the distribution of the data points in statistic) of projected range (R_p), straggle (σ), skewness and kurtosis. Generally, the doping profiles can be obtained by destructive analytical measurement such as secondary ion mass spectroscopy (SIMS) and spreading resistance analysis (SRA). Alternatively, simulation can be done to obtain the doping profile by using different methods such as binary collision approximation (BCA) and molecular dynamic (MD) [37]. The example of simulation programs available has been shown as following in Table 3.1.

Table 3.1 Illustrate the example of simulation programs

Simulator	Author	Technique	Material
TRIM/SRIM	Ziegler	BCA	Amorphous
SUPREM IV		Boltzman	Amorphous
CRYTAL-TRIM	Posselt	BCA	Crystalline/Amorphous
MARLOWE	Robinson	BCA	Crystalline/Amorphous
UT-MARLOWE	Tasch	BCA	Crystalline/Amorphous
UVA-MARLOWE	Arias	BCA	Crystalline/Amorphous
REED	Cai	MD	Crystalline
MDRANGE	Nordlund	MD	Crystalline

There are numerous ion implant simulation programs with different accuracies based on the model (see table 3.1). The SRIM simulation [38] will be used to simulate the as implanted doping profile (without annealing) in the discussion in Chapter 6.

3.1.2 Monte-Carlo based SRIM

Stopping and Range of Ion in Matter (SRIM) simulation is based on Monte-Carlo calculation to simulate the implanted profiles. The basic concept of Monte-Carlo calculation is the simulation of the history of a projectile through its successive collisions with target atoms. The result is based upon the summation of these scattering events occurring along a large number of simulated particle trajectories within the target. The particle with a given energy, position, and direction, is assumed to change direction due to binary nuclear collisions and to move in straight paths between collisions. The doping profile by SRIM simulation is shown in fig 3.3.

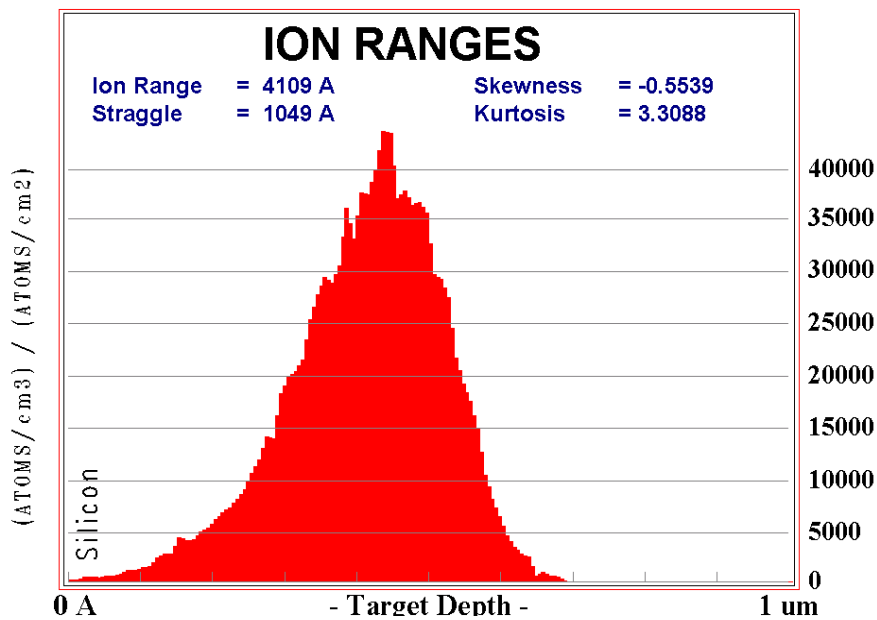


Fig 3.3 Doping profile by using SRIM simulation [38].

SRIM simulation able to predict the projected range and peak concentration of as-implant profile (implant dopant without annealing) with high accuracy. However, the limitation of this program is that the target material is assumed as amorphous, which results in the less effectiveness to predict the "channeling effects" usually observed in crystalline substrates.

3.1.3 Ion implant process

Ion implantation has the advantages over more simple techniques such as driven-in diffusion because of the ability to introduce nearly any kind dopant into the substrate with precise control of the dopant location and the ability to predict the dopant location as well as the distribution.

The implanted dose (Φ in cm^{-2}) is precisely controlled by beam current (I in ampere), and implantation duration (t in second). The implant dosage will determine the total doping concentration in the implant process. Apart from this, the energy of implanted dopant can be controlled to determine the range of the implanted dopant.

Based on the application of implant process, there will be different criteria for implant conditions such as implant energy, angle and dose. There are different type of implanters, such as high-current (HC), medium current (MC), ultra low energy (ULE) and high-energy (HE) implanter designed to achieve desired implant energy and beam current.

The formation of the source/drain and source/drain extension structure (see fig 3.4 and fig 3.5) will involve low energy implant process with high dose. This kind of implant application requires implanter with low energy and high current capabilities. Other cases like threshold voltage adjust implant (V_t implant) and

punchthrough stop implant were generally implanted with medium current implanter on account of their implant depth and dosage. High-energy implant is well recognized for p-well, n-well, retrograde p-well and retrograde n-well implant applications in order to place the dopant in the deep region.

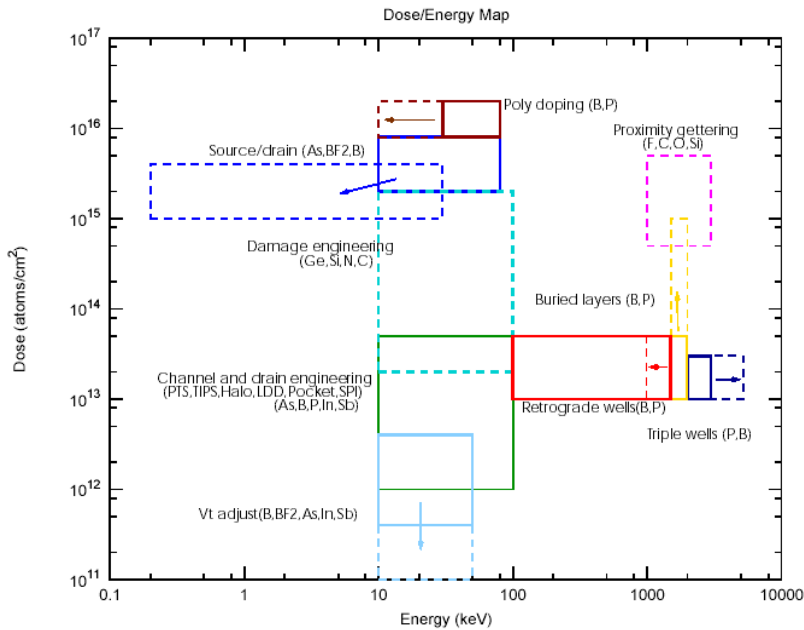


Fig 3.4 Dose and energy requirement of ion implant process depending on the implantation application [34].

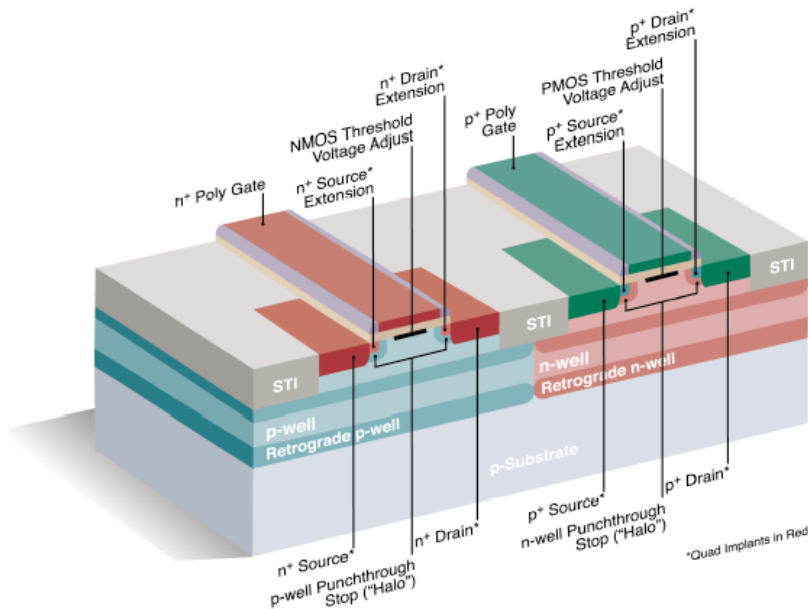


Fig 3.5 The standard CMOS structure [35]

In this work, the implant angle and photoresist shadowing study involves the high-energy implant with the implant depth of 4000Å to 7000Å. This implant process is well recognized as the well application implant and will be performed by using NV-GSD200 HE batch implanter.

3.1.4 Ion implant angle

In ion implant process, the direction of incident beam can be defined by tilt (θ) and twist (Φ) as shown in the fig 3.6(a) below. Tilt (θ) is defined as the angle between the ion beam and the normal to the wafer surface. Meanwhile, twist (Φ) can be defined as the azimuthal angle between the projection of the ion beam on the wafer surface and the [011] crystallographic direction (the direction from the center of the wafer to the wafer notch) [32].

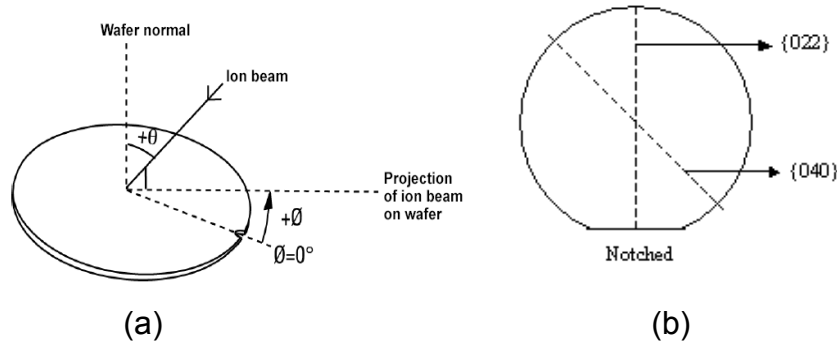


Fig 3.6 (a) Definition of tilt (θ) and twist (Φ) (b) wafer orientation for <100> wafer [2]

Changing the tilt angle for the implant process can be analogy as placing the dopant at different wafer orientation. In semiconductor industry, the production wafer for integrated circuit fabrication will use silicon substrate in the (100) orientation as shown in fig 3.7. Thus, tilt 0° implant will be referring to implant the dopant into silicon wafer with (100) orientation and tilting the implant angle will be referred from this orientation as well.